Interfacial Thermal Conductance Observed to be Higher in Semiconducting than Metallic Carbon Nanotubes

Stephen Dongmin Kang,[†,∥] Seong Chu Lim,[‡,∥] Eui-Sup Lee,[§] Young Woo Cho,[‡] Yong-Hyun Kim,[§] Ho-Ki Lyeo,[†,*] and Young Hee Lee[‡,*]

[†]Korea Research Institute of Standards and Science, Daejeon, 305-340, Republic of Korea, [‡]Department of Physics and Department of Energy Science, Sungkyunkwan Advanced Institute of Nanotechnology, Sungkyunkwan University, Suwon, 440-746, Republic of Korea, and [§]Graduate School of Nanoscience and Technology (WCU), KAIST, Daejeon 305-701, Republic of Korea. [∥]These authors made equal contributions.

ABSTRACT

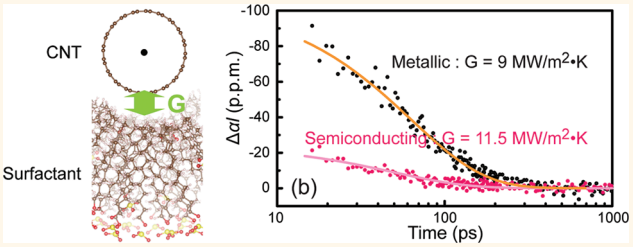

Thermal transport at carbon nanotube (CNT) interfaces was investigated by characterizing the interfacial thermal conductance between metallic or semiconducting CNTs and three different surfactants. We thereby resolved a difference between metallic and semiconducting CNTs. CNT portions separated by their electronic type were prepared in aqueous suspensions. After slightly heating the CNTs dispersed in the suspension, we obtained cooling curves by monitoring the transient changes in absorption, and from these cooling curves, we extracted the interfacial thermal conductance by modeling the thermal system. We found that the semiconducting CNTs unexpectedly exhibited a higher conductance of 11.5 MW/m^2·K than that of metallic CNTs (9 MW/m^2·K). Meanwhile, the type of surfactants hardly influenced the heat transport at the interface. The surfactant dependence is understood in terms of the coupling between the low-frequency vibrational modes of the CNTs and the surfactants. Explanations for the electronic-type dependency are considered based on the defect density in CNTs and the packing density of surfactants.

KEYWORDS: interfacial thermal conductance · thermal boundary resistance · carbon nanotube · TDTR · thermal transport

A peculiar character of single-walled carbon nanotubes (SWCNTs) is found in their electronic properties, where the nanotubes exhibit either a metallic or semiconducting behavior, depending on the chirality of the nanotube.[1] While the two types are obviously distinguished by their electronic properties, whether there is such an appreciable distinction in the thermal transport properties is an interesting question that remains unanswered. On one hand, the thermal conductivity of SWCNTs is extremely high (>3000 W/m·K) regardless of the type,[2,3] where the exceptional transport dominated by lattice vibrations obscures any observable differences between the types. On the other hand, the interfacial thermal conductance at the CNT surface is as low as the interfaces of highly dissimilar solids,[4−6] making it a rate-determining property, which gives a better chance for measurements to resolve a difference between the two electronic types if there is any.

Recent advances in the technology of CNTs further motivate investigation into these type-dependent thermal transport properties. Now separated portions of metallic and semiconducting CNTs can be readily prepared[7] and are commercially available. Moreover, numerous applications require a specific type of CNTs, metallic or semiconducting, for device performance, which demands the respective thermal characterization of each type. For instance, CNT bumps for interconnect applications exploit the thermal conducting property of CNTs while also requiring metallic electrical conduction;[8] enhancements in the efficiency of photovoltaic devices are achieved by using only semiconducting CNTs for the collector composite, while an improved thermal stability is also expected due to the CNTs.[9]

In such applications where it is desired to exploit the high thermal conductivity of CNTs, what becomes important for the thermal management performance of the CNT-incorporated systems is the interaction between the CNTs and their surrounding environment. The interaction is now well recognized to be weak enough to limit the overall thermal transport in the system.[10,11] This "inert" behavior of CNTs has drawn attention to the interface property of CNTs, which is characterized

* Address correspondence to hklyeo@kriss.re.kr; leeyoung@skku.edu.

Received for review December 20, 2011 and accepted April 2, 2012.

Published online April 02, 2012
10.1021/nn2049762

by the interfacial thermal conductance G. G determines the heat flux J across an interface for a discontinuous temperature drop ΔT through the relationship $J = -G\Delta T$. The reciprocal $1/G$ is often referred to as the thermal boundary resistance.[12]

Comparative characterization of the interfacial thermal conductance G for metallic and semiconducting CNTs has not yet been rewarding.[13] In fact, experimental measurements of G on *individually isolated* CNTs are rare by themselves in the literature, once we leave out the indirect estimations from electrical breakdowns.[13−15] Thus, references to the G value of CNTs rely heavily on an early study conducted by Huxtable *et al.*[4] In their study, single-walled CNTs were dispersed with sodium dodecyl sulfate (SDS) in water, and, from transient absorption measurements, the conductance was determined as $G \approx 12$ MW/m^2·K for the CNT−SDS interface. This G value indicates that the single interface is equivalent, in terms of thermal resistance, to a SiO_2 insulation layer of more than 100 nm. While their study directly identified the thermally inert character of CNTs, the effect of metallicity has not been discussed. Estimations of G have been attempted in many other works, computationally[10,16−19] as well as experimentally from arrays[20,21] and composites.[22−24] Yet, the impact of the metallicity of CNTs has not been considered. Presently, theories on the interfacial conductance lead us to an expectation that the metallicity of the CNTs would be, at most, an additive route to the thermal coupling with the surroundings; some reports suggest electron−phonon coupling mechanisms at metal−nonmetal interfaces;[25] otherwise, the electronic contribution has been generally considered negligible.[10,16−19]

In this work, we present experimental results contrary to the general expectation. We measured the interfacial thermal conductance of SWCNTs separated by their metallicity and dispersed in a water solution with various surfactants. An unexpected behavior in the interfacial heat flow of SWCNTs, with a higher conductance not in the metallic but in the semiconducting SWCNTs, is found. We also investigated the effect of the surfactant types to assess the role of the surrounding matrix on the heat flow, which provides a basis for understanding the results from metallic and semiconducting SWCNTs.

RESULTS AND DISCUSSION

Preparation and Characterization of the SWCNT Suspensions. Metallic (m-) and semiconducting (s-) SWCNTs, of the same average diameter of ~1.4 nm, were dispersed in aqueous suspensions using the following surfactants: sodium dodecyl sulfate, sodium cholate (SC), and sodium dodecylbenzenesulfonate (SDBS). The prepared solutions are displayed in Figure 1a. The suspensions are distinguished by their optical absorption; samples with m-CNTs appear in a cyan color, while those with s-CNTs appear in a dark reddish color. The difference is apparent in the absorption spectra shown in Figure 1b. The absorption peak for m-CNTs appeared at the wavelength of ~700 nm (M_{11}), while that for s-CNTs appeared at ~1030 nm (S_{22}). On the other hand, the type of surfactants did not affect the absorption wavelength.

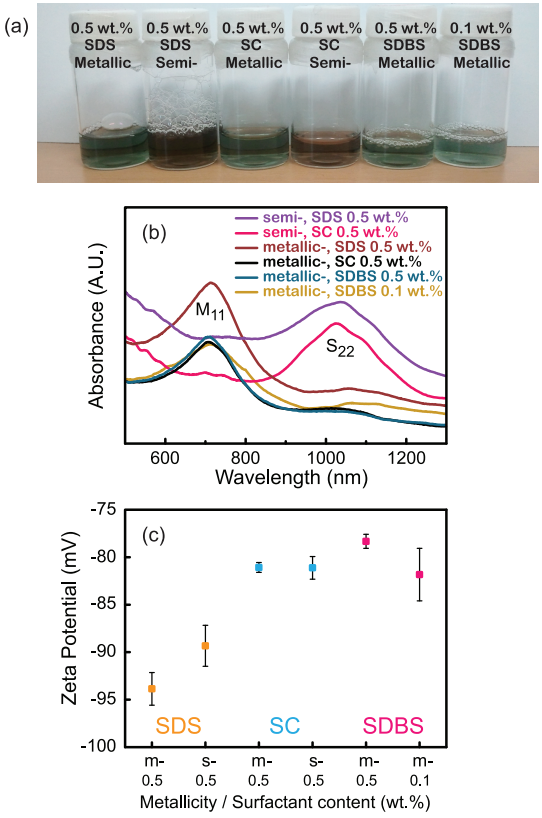

Figure 1. Optical absorption of the suspensions, dependent on the electronic type of the CNTs, shown in (a) the photograph of the samples and (b) the absorption spectra. Absorption peaks representing metallic (M_{11}) and semiconducting (S_{22}) CNTs are labeled in the figure. (c) Zeta potentials measured for each sample.

Large amounts of surfactants were adsorbed on the CNT surface, indicated by the largely negative zeta potentials (<−75 mV) measured in all samples, as shown in Figure 1c; the magnitude of the zeta potential is a rough measure of the amount of surfactants adsorbed on the surface. We note that the surfactant concentration is well above the critical micelle concentration in all samples. The zeta potentials imply that the amounts of SC molecules adsorbed on m-CNTs and s-CNTs are similar, while SDS molecules are absorbed more on m-CNTs.[26]

Interfacial Thermal Conductance of SWCNTs from Transient Absorption Measurements. To measure the interfacial thermal conductance of the CNT surface, we obtained the "cooling curves" for CNTs, curves showing the temperature evolution in the CNTs after an instantaneous heating; we make use of the thermo-optical property of materials where the absorption coefficient α changes linearly for small temperature changes.[4]

We monitored the time-resolved changes in the optical absorption of CNT suspensions after heating with a pulsed pump beam. With the selected wavelength of 740–800 nm, the CNTs are heated by a few degrees Kelvin, while the surfactants and water solution are heated negligibly. The temperature of the CNTs decays over time as they equilibrate with the solution, yielding a transient change in the absorption according to the opto-thermal property of CNTs. The change in absorption was measured by a probe beam as a function of pump-to-probe delay time, giving cooling curves for the CNTs as shown in Figure 2.

The interfacial thermal conductance G of CNTs mainly determines the shape of the cooling curves, which allows us to extract the G value by thermal modeling. Because the low G value for CNTs controls the total heat flow of the system, most of the transient temperature drop occurs at the CNT–surfactant interface, as schematically depicted in Figure 2a. The system is modeled by assuming a two-dimensional system with cylindrical symmetry, which is justified since the thermal transport property along the CNT axis is more conductive by a few orders of magnitude compared to the resistive and rate-determining transport property across the CNT surface. By modeling the dynamics of this system, we fit the calculated curves to the measured data to determine the G values of the CNTs.

The G value determined by model fitting was G = 9 MW/m^2·K for m-CNTs and G = 11.5 MW/m^2·K for s-CNTs, being higher for s-CNTs by ~28%. This difference is much larger than the standard deviation, ~6%, found in the set of repeated measurements. The results were identical for both the CNT–SC (Figure 2b) and CNT–SDS (Figure 2c) interfaces. The extracted G value depends on how the areal heat capacity of CNTs is assumed, which, in this case, was taken from the value of graphite (0.56 mJ/m^2·K). Taking the experimental value from ref 27 yields a lower areal heat capacity (0.46 mJ/m^2·K), which gives lower G values. The results are summarized in Table 1. It should be noted that the heat capacity difference for m- and s-CNTs is negligible.[28]

In a previous study, Huxtable *et al.* obtained, from CNT suspensions prepared with no control on metallicity (single-walled, produced by the HiPCO method), a value of G = 12 MW/m^2·K, which is similar to that obtained from our s-CNT samples.[4] However, in contrast to their analysis in which the cooling curve was fitted to an exponential curve with two decay-time constants, we analyzed our data by thermal modeling, which yields an exponential-like decay function with a single time constant (see Methods and Supporting Information). On the other hand, compared to the G values obtained from CNTs on SiO_2 solid substrates, which range around 12–120 MW/m^2·K when scaled to room temperature,[13] the values obtained in our suspensions (9–11.5 MW/m^2·K) are smaller (up to an order of magnitude).

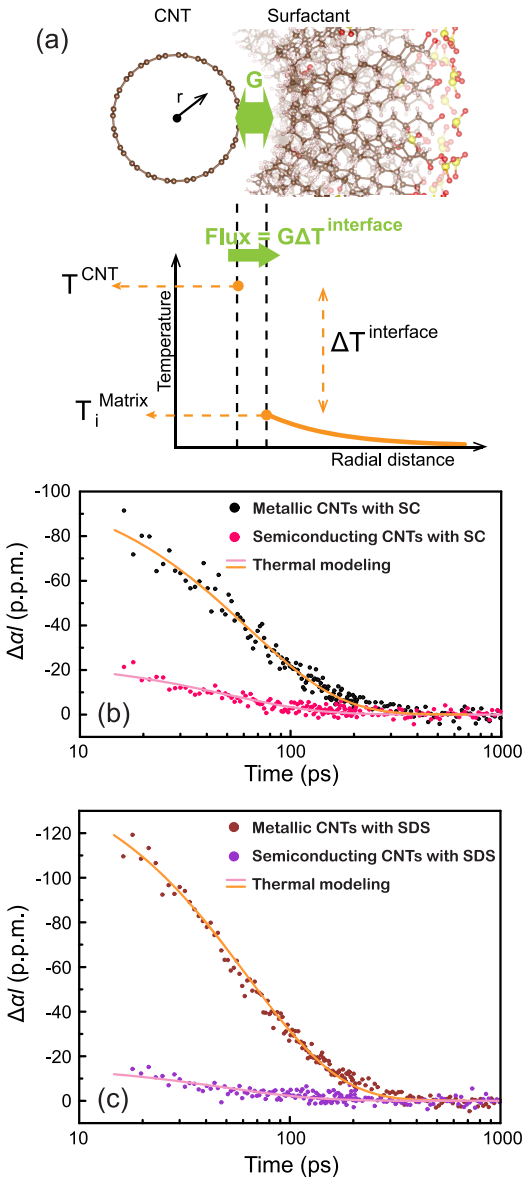

Figure 2. (a) Schematic of the CNT–surfactant system (upper) and the corresponding radial temperature profile in the system (lower). The vibrational coupling at the CNT–surfactant interface is responsible for the interfacial heat flow, which is the rate-determining part for the overall heat transport in the system. A large temperature discontinuity ($\Delta T^{interface}$) is induced at the interface, indicating the resistive property of the interface. (b and c) Cooling curves of metallic and semiconducting CNTs shown by the transient changes in optical absorption after heating with laser pulses. The CNTs were dispersed with (b) SC and (c) SDS. α is the absorption coefficient and l is the path length of the CNT solution (200 μm). The solid lines are calculated from a thermal model and fitted to the data. The interfacial thermal conductance values extracted by thermal modeling are summarized in Table 1. The wavelength of the laser used for measurements was 740 nm, and the surfactant content was 0.5 wt % of the solution for all samples. The signal in the shorter time scale (<15 ps) reflects the photobleaching and cooling of the excited electrons (see refs 4 and 45).

It is rather a peculiar result to find a larger interfacial thermal conductance in s-CNTs than m-CNTs. Under the conventional understanding it is unlikely that the

TABLE 1. Interfacial Thermal Conductance Values Extracted by Thermal Modeling

CNT type	interfacial thermal conductance (MW/m^2·K)
metallic	9[a] (7.5[b])
semiconducting	11.5[a] (9.5[b])

[a] By assuming 0.56 mJ/m^2·K for the areal heat capacity. [b] By assuming 0.46 mJ/m^2·K for the areal heat capacity.

electrical conducting property of the CNTs would contribute to the interfacial thermal conductance since the surfactants are electrically nonconducting. Although we consider electron–phonon coupling mechanisms suggested for metal–nonmetal interfaces,[25] these routes are supposed to be in addition to the vibrational coupling process, which would favor higher conductance in m-CNTs.

Another observation from the results in Figure 2b,c is that the interfacial thermal conductance G appeared independent of the type of the surfactant in both cases for m-CNTs and s-CNTs. We also obtained the cooling curves from m-CNTs dispersed with SDBS, shown together with the SC- and SDS-stabilized samples in Figure 3a. The normalized curves from three different surfactants all fit to a single curve, explicitly indicating the same G value within the sensitivity of our measurements, which is ~0.5 MW/m^2·K. The surfactant-independent values suggest that the different G values of m-CNTs and s-CNTs are likely to reflect the character of the CNTs rather than the surfactants.

We note that the stronger excitation signal ($\Delta\alpha l$) from m-CNTs than s-CNTs is due to the relatively sensitive thermo-optical property of m-CNTs, but is not the result of any differences in the thermal properties. In other words, m-CNTs exhibit a larger change in absorption than s-CNTs for a given temperature change. To compensate for the smaller excitation signal ($\Delta\alpha l$) from s-CNTs, we elongated the optical path l of the sample (*i.e.*, the thickness of the sample container); still, this did not change the measured value of interfacial thermal conductance (see the Supporting Information). This also confirms that the signal strength from our s-CNT samples, while smaller than that from m-CNTs, is sufficiently large for analysis.

The thermal decaying behavior was independent of the concentration of the surfactant added to the CNT solution, as long as the added amount exceeded the critical micelle concentration (CMC). Shown in Figure 3b are the cooling curves of m-CNTs dispersed with 0.1 and 0.5 wt % of SDBS, which are both well above the CMC. The identical cooling behavior shown in this plot indicates that, above the CMC, the surfactants are sufficiently saturated at the CNT surface to probe the interface thermal property. The thermal decaying behavior also did not depend on the wavelength, λ, of the laser beams in the range 740 < λ < 800 nm. Shown in

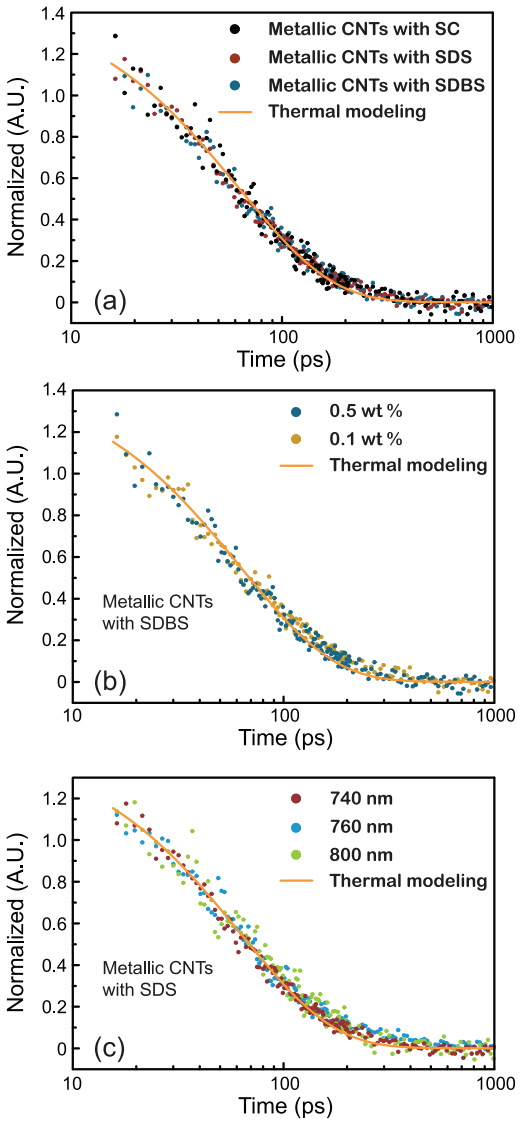

Figure 3. Cooling curves of metallic CNTs measured under different conditions and drawn on a normalized scale: (a) dispersed with different surfactants (SC, SDS, and SDBS); (b) dispersed with different amounts of surfactants (SDBS); (c) measured by using laser beams of different wavelengths. For all samples, the surfactant content was 0.5 wt % and the wavelength used was 740 nm unless mentioned otherwise. The calculated curve and data points of metallic CNTs with SC and SDS in (a) are scaled from the data in Figure 2b,c, respectively; data points for 0.5 wt % in (b) are identical to the SDBS data in (a) (navy blue color); data points for 740 nm in (c) are identical to the SDS data in (a) (brown color).

Figure 3c are the cooling curves of SDS-stabilized m-CNTs measured at different wavelengths, confirming that the curves represent the thermal cooling of CNTs but not any kind of specific absorption.

Thermal Coupling at the SWCNT–Surfactant Interface. The thermal transport phenomena observed at the CNT–surfactant interface can be understood in terms of the coupling between the vibrational modes at the interface, which should be responsible for the thermal conductance at the CNT–surfactant interface. This

coupling mechanism can be roughly visualized by frequency-wise matching the vibrational spectrum of each side of the interface, as drawn in Figure 4. Under the harmonic picture, vibrational mode coupling takes place between the vibrational modes with the same frequencies. For the interactions with the molecule matrix environment at room temperature, the harmonic picture provides an approximate, but basic, frame to understand the interfacial interactions,[29] which also reveals the need to consider anharmonic routes. We begin our discussions based on the picture of harmonic interactions at the interface.

The extremely low value of G implies that the vibrational coupling at the CNT−surfactant interface is only effective at a limited frequency range among the vibrational spectrum. The upper limit of this frequency range can be appreciated by considering the phonon radiation limit[5,12] of the interfacial thermal conductance, which is given by

$$G_{rad} = \frac{\pi k_b \nu_{upper}^3}{c_D^2} \quad (1)$$

where ν_{upper} is the upper limit of the vibrational frequency involved in the coupling, c_D the Debye velocity, and k_b the Boltzmann constant. This phonon radiation limit G_{rad} is the maximum conductance of an interface when the incident energy of phonons is fully transmitted across a harmonically coupled interface. Conventionally, this equation is used to evaluate G_{rad} when the vibrational spectrum of one side of the interface is limited by the vibrational cutoff frequency, while, in the present case, we use the equation to estimate the upper frequency limit of the coupled vibrational modes, ν_{upper}, for a given G value. For the Debye velocity, we consider the group velocity of the flexure modes in SWCNTs, which dominate the CNT−surfactant interactions.[10] The dispersion relation of the flexure modes exhibits a quadratic behavior at long wavelengths,[30] so we take the maximum value ($c_D \approx 7.2$ nm/ps) to obtain the upper limit of the frequency. Then, the previously determined G = 11.5 MW/m^2·K yields ν_{upper} = 2.4 THz. This estimation gives a grasp on the effective frequency range where vibrational interactions are actively taking place. Physically, ν_{upper} is limited by the strength of the interaction between the CNT and the surfactants, which is a weak van der Waals interaction (see Figure S2 in the Supporting Information). We note that ν_{upper} is an estimate for a harmonic process; it does not take into account other parallel routes such as inelastic scattering events at the interface.[31]

In addition to the narrow frequency window for vibrational mode coupling, the vibrational spectrum below ν_{upper} is not very specific to the type of surfactants, explaining why the thermal decay curves of CNTs with different surfactants yield a similar value of G. Shown in Figure 4b−e is the calculated vibrational

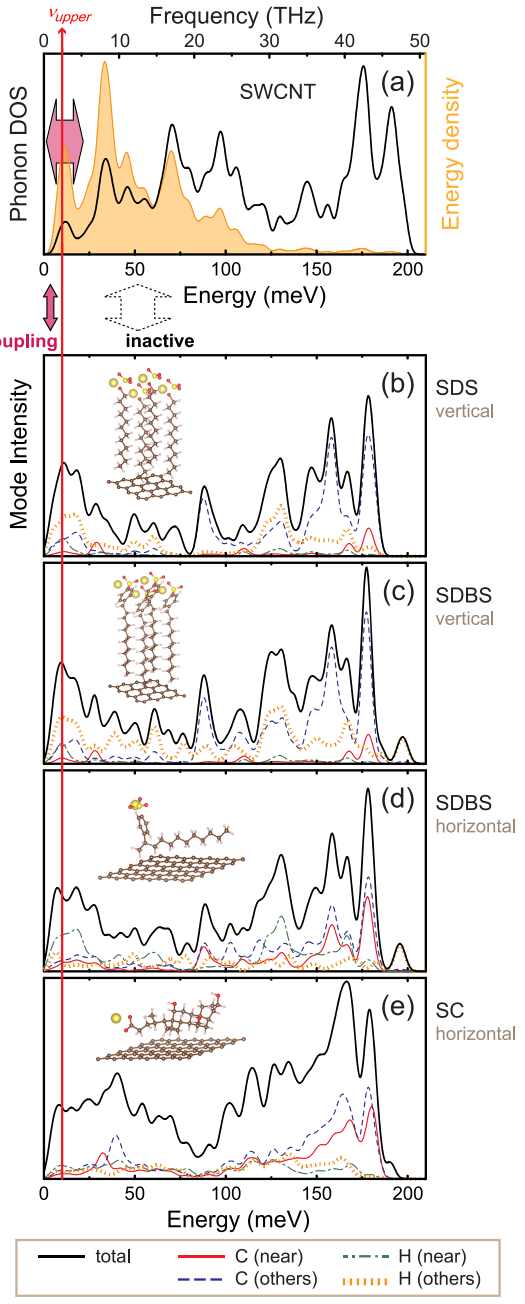

Figure 4. Vibrational mode coupling process between CNTs and surfactants depicted by comparing the vibrational states with respect to their frequencies. (a) Calculated phonon density of states of a (10,10) SWNT. The color shade shows the spectral distribution of thermal energy among phonon frequencies at 300 K. (b−e) Calculated vibration spectra for surfactants adsorbed on a flat-carbon surface (graphene). The states of graphene have been excluded from the spectra. The adsorption structures described by the calculation model are shown in the inset of the spectra. The relative contributions from the vibrational states of the constituent atoms are also indicated as colored lines; "near" denotes atoms near the adsorption surface, while "others" denotes those that are far. The vibrational mode coupling process between CNTs and surfactants is active at low frequencies, but not effective at high frequencies. The distinction of these frequency regimes is roughly estimated as $\nu_{upper} \approx$ 2.4 THz (10 meV) from the phonon radiation limit. The internal coupling within the CNTs between high- and low-frequency phonons, drawn as a double-sided arrow within the CNT spectrum, depicts the alternative route for the heat dissipation of the high-frequency phonons in the CNTs.

density of states (DOS) for surfactants adsorbed on a flat carbon surface, *i.e.*, graphene. Comparing the spectra shows that the DOS of vertically adsorbed SDBS is more similar to that of vertically adsorbed SDS rather than horizontally adsorbed SDBS. To generalize, the low- to moderate-frequency DOS of the surfactants depends more on factors such as the geometrical folding or adsorption structure of the surfactants than the chemical bondings within the molecule. The low-frequency DOS below ν_{upper} particularly exhibits such a dependency. Therefore, as long as the CNT–surfactant interaction strength is similar, the interfacial thermal conductance would be independent of the surfactant type.

Anharmonic Processes of the Phonons in SWCNTs. While the frequency limit ν_{upper} was a rough estimation for the harmonic process at the interface, the conclusions are supported by molecular dynamics studies,[10,18] which suggest that, in CNTs, the active coupling of the phonons with the environment (*i.e.*, fast heat transport) is indeed limited to the low-frequency phonons. However, the spectral distribution of thermal energy in CNTs, shown in Figure 4a, implies that the phonons above ν_{upper} still need a route for heat dissipation, calling for the need to consider the anharmonic process of phonons.

Brought to attention by the low-frequency-limited coupling of the vibrational modes at the CNT surface is an anharmonic coupling mechanism: the internal coupling between phonon modes within the CNTs. At room temperature, the majority of the thermal energy in the CNTs is distributed at phonon frequencies higher than ν_{upper}, with its main portion reaching up to 25–30 THz (Figure 4a). In order for the CNTs to reach thermal equilibrium with the surrounding matrix, the thermal energy in both the low- and high-frequency phonon modes needs a channel to dissipate heat. Because of the narrow coupling channel at low frequency, the thermal energy in the high-frequency modes should be dissipated through anharmonic internal phonon coupling between the high- and low-frequency phonons within the CNTs. In previous reports[4,10,18] it was suggested that this process determines the interfacial thermal conductance at the CNT surface.

On the basis of this argument that the determining factor for the interfacial thermal conductance G of CNTs is the internal phonon coupling process, we account for the unexpectedly higher G of s-CNTs: the higher defect density in s-CNTs provides more sources for the internal phonon coupling. Lattice defects serve as an effective kernel for the previously discussed anharmonic process for high-frequency phonons since lattice defects mostly scatter the high-frequency phonons. The density of these lattice defects depends on the chirality of the CNTs since the energy cost for formation depends on the curvature of the carbon lattice. Our calculations on the formation energy, summarized in Table 2, show that monovacancies are less favorable in armchair-type CNTs; these types are supposed to be the majority in our m-CNT samples.[32–35] Then, s-CNTs should exhibit a higher interfacial thermal conductance than m-CNTs. The formation energy for double vacancies or Stone–Wales defects also has a similar dependency.[36] Still, it should be noted that this argument takes into account that our m-CNT samples are supposedly abundant in armchair types, which makes our argument more based on the chirality but not the metallicity of CNTs; solely focusing on the effect of the metallicity could also yield opposing arguments.[36] We also add that, unfortunately, probing the D band to G band ratio with Raman spectroscopy to compare the defect density is not possible in the present case since it is more dependent on the chirality of the CNTs than the defect density.[37,38]

TABLE 2. Calculated Formation Energies for Monovacancies in CNTs

CNT type				
electronic	type	(*n*,*m*)	diameter (nm)	monovacancy formation energy (eV)
metallic	armchair	(10,10)	1.36	6.50
	zigzag	(18,0)	1.41	6.19
semiconducting		(17,0)	1.33	6.17

We find that most of the other possibilities provide only a limited explanation for the higher conductance observed in s-CNTs. A denser packing in the matrix of surfactants surrounding m-CNTs could suppress the low-frequency vibrational DOS on the surfactant side,[39] which may result in a lower interfacial conductance. In fact, it is known that SDS molecules form a higher packing density on m-CNTs,[26] as was also confirmed by our zeta potential measurements (Figure 1c). However, our zeta potential measurements on CNTs dispersed with SC do not show such a dependency on metallicity.[40] Above all, the surfactant-independent behavior of the thermal decay for both s- and m-CNTs rules out many possibilities regarding any differences in the surfactants. Looking at the CNT side, it is known that the chiral angle barely affects the phonon DOS, particularly at low frequencies,[41] which also rules out many explanations.

CONCLUSIONS

The interfacial thermal conductance G at the CNT–surfactant surface was observed to be higher in s-CNTs (11.5 MW/m^2·K) than in m-CNTs (9 MW/m^2·K). The G values were obtained from transient absorption measurements on CNT suspensions, followed by model fitting. Changing the surfactant to various types (SC, SDS, SDBS) did not influence our results. Supposing that G is determined by the internal phonon

coupling between high- and low-frequency phonons within the CNTs, we find that a higher defect density in s-CNTs explains our results. The calculated defect-formation energy in CNTs supports our argument.

Nevertheless, thus far, the issue of s-CNTs exhibiting higher interfacial thermal conductance than m-CNTs seems not yet sufficiently elucidated. The tentative arguments provided in this report may benefit from future studies, *e.g.*, measurements from surfactant-free dispersions of CNTs in solid matrices. We also add that we are cautious in considering our results showing the surfactant independence as an experimental validation of the rate-determining interpretation of the internal phonon coupling within the CNTs. Although the surfactant independence has been suggested in ref 4 based on this interpretation, and our results conform to the prediction, our argument with the vibrational DOS of the surfactants shows that the rate-determining interpretation is not a necessary prerequisite; similar interaction strengths and a nonspecific vibrational DOS may suffice to explain the surfactant independence.

METHODS

Sample Preparation. Metallic and semiconducting SWCNTs of >95% purity, produced by the arc discharge method, were purchased from NanoIntegris Inc. The SWCNTs were rinsed with methanol to remove the residual surfactants, followed by examination with transmission electron microscopy to check the removal. Then we added 1 mg of the purified SWCNTs into a 40 mL aqueous solution in which 40 or 200 mg of surfactants was dissolved in advance. The surfactants were either SC, SDS, or SDBS. To promote the debundling of the SWCNTs, the solutions were agitated using a horn-type homogenizer run in 3 min on and 2 min off cycles. The remaining bundles were removed by centrifugation at 10 000 rpm for 30 min.

Transient Absorption Measurements. A pump–probe method was used to heat the CNTs and measure the transient changes in absorption. A train of subpicosecond laser pulses was produced by a Ti:sapphire mode-locked laser at a repetition rate of 75.8 MHz and split into pump and probe beams. The pump and probe beams were modulated by an electro-optic modulator at a frequency of 9.77 MHz and by a mechanical chopper at a frequency of 250 Hz, respectively. The delay time between the two beams was adjusted by a mechanical delay stage. The beams were transmitted through the solution sample, and the transmitted probe beam was detected by a photodetector. The in-phase signal was picked out by an RF lock-in amplifier, which reflects the transient changes in the sample absorption.

Thermal Modeling. The temperature change of the CNTs was analyzed by solving the heat equations for the CNT suspension system subject to periodic heating. Solving the equations is substantially simplified by solving them in the frequency domain. The frequency domain solution for the temperature in the CNTs turns out as

$$\frac{1}{\Delta T^{CNT}} = \frac{1}{P}\left[i\omega C_A + \frac{1}{\frac{1}{G} + \frac{1}{\Lambda_{mat} q_{mat}} \frac{K_0(q_{mat} r_i)}{K_1(q_{mat} r_i)}} \right] \quad (2)$$

where C_A is the areal heat capacity of the CNT, G the interfacial thermal conductance at the CNT interface, P the areal density of power, Λ_{mat} the thermal conductivity of the surrounding matrix, and r_i the radial distance from the center of the CNT to the CNT–matrix interface. q_{mat} is defined as ${q_{mat}}^2 = i\omega C_{mat}/\Lambda_{mat}$, where C_{mat} is the volumetric heat capacity of the surrounding matrix. K is the modified Bessel function. The cooling curve can be obtained by transforming this solution to the time domain. (Details on the thermal modeling can be found in the Supporting Information.)

First-Principles Calculations. For first-principles density-functional theory calculations, we employed the projector-augmented wave potentials[42] with a plane-wave basis set and the Perdew–Burke–Ernzernhof exchange–correlation functional[43] as implemented in the Vienna *Ab-Initio* Simulation Package[44] code. For geometry optimization, we used a kinetic energy cutoff of 400 eV and Gaussian smearing of 0.05 and 0.1 eV for semiconducting and metallic CNTs, respectively. We also used a van der Waals correction for the interaction between graphene and surfactants. The formation energy of the defects was calculated using a $(1 \times 1 \times 2)$ k-point sampling for supercells of $(1 \times 1 \times 5)$ (17, 0), $(1 \times 1 \times 5)$ (18, 0), and $(1 \times 1 \times 9)$ (10, 10) carbon nanotubes with a vacuum separation of 15 Å. The vibrational spectra were calculated using $(24 \times 24 \times 1)$ equilibrium k-points for supercells of individual surfactants relaxed either on a $(2 \times 2 \times 1)$ or $(6 \times 6 \times 1)$ graphene sheet. The vacuum separation was 15 Å. All atomic forces were minimized to <0.025 eV/Å, and any in-plane stresses were fully relaxed. Gaussian smearing of 2.5 meV was used for plotting the phonon density of states.

Conflict of Interest: The authors declare no competing financial interest.

Acknowledgment. The authors thank Dr. Ki-Jeong Kong for preliminary calculations. S.D.K. and H.-K.L. were supported by the Converging Research Center Program of MEST (2011K000617). S.C.L., Y.W.C., and Y.H.L. were supported by the WCU program (R31-2008-000-10029-0) of NRF/MEST and the Star Faculty program (2010-0029653).

Supporting Information Available: Additional information and figures. This material is available free of charge *via* the Internet at http://pubs.acs.org.

REFERENCES AND NOTES

1. Saito, R.; Dresselhaus, G.; Dresselhaus, M. S. *Physical Properties of Carbon Nanotubes*; World Scientific Publishing Company: Singapore, 1998.
2. Yu, C.; Shi, L.; Yao, Z.; Li, D.; Majumdar, A. Thermal Conductance and Thermopower of an Individual Single-Wall Carbon Nanotube. *Nano Lett.* **2005**, *5*, 1842–1846.
3. Pop, E.; Mann, D.; Wang, Q.; Goodson, K.; Dai, H. Thermal Conductance of an Individual Single-Wall Carbon Nanotube above Room Temperature. *Nano Lett.* **2006**, *6*, 96–100.
4. Huxtable, S. T.; Cahill, D. G.; Shenogin, S.; Xue, L.; Ozisik, R.; Barone, P.; Usrey, M.; Strano, M. S.; Siddons, G.; Shim, M.; *et al.* Interfacial Heat Flow in Carbon Nanotube Suspensions. *Nat. Mater.* **2003**, *2*, 731–734.
5. Lyeo, H.-K.; Cahill, D. G. Thermal Conductance of Interfaces between Highly Dissimilar Materials. *Phys. Rev. B* **2006**, *73*, 144301.
6. Pop, E. Energy Dissipation and Transport in Nanoscale Devices. *Nano Res.* **2010**, *3*, 147–169.
7. Arnold, M. S.; Green, A. A.; Hulvat, J. F.; Stupp, S. I.; Hersam, M. C. Sorting Carbon Nanotubes by Electronic Structure Using Density Differentiation. *Nat. Nanotechnol.* **2006**, *1*, 60–65.
8. Iwai, T.; Shioya, H.; Kondo, D.; Hirose, S.; Kawabata, A.; Sato, S.; Nihei, M.; Kikkawa, T.; Joshin, K.; Awano, Y. *et al. Thermal and Source Bumps Utilizing Carbon Nanotubes for Flip-Chip High Power Amplifiers 2005 IEEE International Electron Devices Meeting; Technical Digest*; **2005**; December, pp 257–260.
9. Dang, X.; Yi, H.; Ham, M.-H.; Qi, J.; Yun, D. S.; Ladewski, R.; Strano, M. S.; Hammond, P. T.; Belcher, A. M. Virus-Templated

Self-Assembled Single-Walled Carbon Nanotubes for Highly Efficient Electron Collection in Photovoltaic Devices. *Nat. Nanotechnol.* **2011**, *6*, 377–384.
10. Shenogin, S.; Xue, L.; Ozisik, R.; Keblinski, P.; Cahill, D. G. Role of Thermal Boundary Resistance on the Heat Flow in Carbon-Nanotube Composites. *J. Appl. Phys.* **2004**, *95*, 8136–8144.
11. Kang, S. D.; Yoo, J. J.; Lyeo, H.-K.; Song, J. Y.; Lee, S.; Yu, J. Assessing the Thermal Conductivity of Non-uniform Thin-films: Nanocrystalline Cu Composites Incorporating Carbon Nanotubes. *J. Appl. Phys.* **2011**, *110*, 023506.
12. Swartz, E. T.; Pohl, R. O. Thermal Boundary Resistance. *Rev. Mod. Phys.* **1989**, *61*, 605–668.
13. Liao, A.; Alizadegan, R.; Ong, Z.-Y.; Dutta, S.; Xiong, F.; Hsia, K. J.; Pop, E. Thermal Dissipation and Variability in Electrical Breakdown of Carbon Nanotube Devices. *Phys. Rev. B* **2010**, *82*, 205406.
14. Maune, H.; Chiu, H.-Y.; Bockrath, M. Thermal Resistance of the Nanoscale Constrictions between Carbon Nanotubes and Solid Substrates. *Appl. Phys. Lett.* **2006**, *89*, 013109.
15. Tsai, C.-L.; Liao, A.; Pop, E.; Shim, M. Electrical Power Dissipation in Semiconducting Carbon Nanotubes on Single Crystal Quartz and Amorphous SiO_2. *Appl. Phys. Lett.* **2011**, *99*, 053120.
16. Zhong, H.; Lukes, J. R. Interfacial Thermal Resistance between Carbon Nanotubes: Molecular Dynamics Simulations and Analytical Thermal Modeling. *Phys. Rev. B* **2006**, *74*, 125403.
17. Prasher, R. Thermal Boundary Resistance and Thermal Conductivity of Multiwalled Carbon Nanotubes. *Phys. Rev. B* **2008**, *77*, 075424.
18. Carlborg, C. F.; Shiomi, J.; Maruyama, S. Thermal Boundary Resistance between Single-Walled Carbon Nanotubes and Surrounding Matrices. *Phys. Rev. B* **2008**, *78*, 205406.
19. Ong, Z.-Y.; Pop, E. Molecular Dynamics Simulation of Thermal Boundary Conductance between Carbon Nanotubes and SiO_2. *Phys. Rev. B* **2010**, *81*, 155408.
20. Panzer, M. A.; Zhang, G.; Mann, D.; Hu, X.; Pop, E.; Dai, H.; Goodson, K. E. Thermal Properties of Metal-Coated Vertically Aligned Single-Wall Nanotube Arrays. *J. Heat Transfer* **2008**, *130*, 052401.
21. Cola, B. A.; Xu, J.; Fisher, T. S. Contact Mechanics and Thermal Conductance of Carbon Nanotube Array Interfaces. *Int. J. Heat Mass Transfer* **2009**, *52*, 3490.
22. Bryning, M. B.; Milkie, D. E.; Islam, M. F.; Kikkawa, J. M.; Yodh, A. G. Thermal Conductivity and Interfacial Resistance in Single-Wall Carbon Nanotube Epoxy Composites. *Appl. Phys. Lett.* **2005**, *87*, 161909.
23. Bui, K.; Grady, B. P.; Papavassiliou, D. V. Heat Transfer in High Volume Fraction CNT Nanocomposites: Effects of Inter-Nanotube Thermal Resistance. *Chem. Phys. Lett.* **2011**, *508*, 248–251.
24. Marconnet, A. M.; Yamamoto, N.; Panzer, M. A.; Wardle, B. L.; Goodson, K. E. Thermal Conduction in Aligned Carbon Nanotube-Polymer Nanocomposites with High Packing Density. *ACS Nano* **2011**, *5*, 4818–4825.
25. Mahan, G. D. Kapitza Thermal Resistance Between a Metal and a Nonmetal. *Phys. Rev. B* **2009**, *79*, 075408.
26. Niyogi, S.; Densmore, C. G.; Doorn, S. K. Electrolyte Tuning of Surfactant Interfacial Behavior for Enhanced Density-Based Separations of Single-Walled Carbon Nanotubes. *J. Am. Chem. Soc.* **2008**, *131*, 1144–1153.
27. Hone, J.; Batlogg, B.; Benes, Z.; Johnson, A. T.; Fischer, J. E. Quantized Phonon Spectrum of Single-Wall Carbon Nanotubes. *Science* **2000**, *289*, 1730–1733.
28. Mizel, A.; Benedict, L. X.; Cohen, M. L.; Louie, S. G.; Zettl, A.; Budraa, N. K.; Beyermann, W. P. Analysis of the Low-Temperature Specific Heat of Multiwalled Carbon Nanotubes and Carbon Nanotube Ropes. *Phys. Rev. B* **1999**, *60*, 3264.
29. Segal, D.; Nitzan, A.; Hanggi, P. Thermal Conductance Through Molecular Wires. *J. Chem. Phys.* **2003**, *119*, 6840.
30. Mahan, G. D.; Jeon, G. S. Flexure Modes in Carbon Nanotubes. *Phys. Rev. B* **2004**, *70*, 075405.
31. Hopkins, P. E.; Duda, J. C.; Norris, P. M. Anharmonic Phonon Interactions at Interfaces and Contributions to Thermal Boundary Conductance. *J. Heat Transfer* **2011**, *133*, 062401.
32. Ding, F.; Harutyunyan, A. R.; Yakobson, B. I. Dislocation Theory of Chirality-Controlled Nanotube Growth. *P. Natl. Acad. Sci.* **2009**, *106*, 2506–2509.
33. Hirahara, K.; Kociak, M.; Bandow, S.; Nakahira, T.; Itoh, K.; Saito, Y.; Iijima, S. Chirality Correlation in Double-Wall Carbon Nanotubes as Studied by Electron Diffraction. *Phys. Rev. B* **2006**, *73*, 195420.
34. Cowley, J. M.; Nikolaev, P.; Thess, A.; Smalley, R. E. Electron Nano-Diffraction Study of Carbon Single-Walled Nanotube Ropes. *Chem. Phys. Lett.* **1997**, *265*, 379–384.
35. Rao, R.; Liptak, D.; Cherukuri, T.; Yakobson, B. I.; Maruyama, B. *In Situ* Evidence for Chirality-Dependent Growth Rates of Individual Carbon Nanotubes. *Nat. Mater.* **2012**, *11*, 213–216.
36. Carlsson, J. M. Curvature and Chirality Dependence of the Properties of Point Defects in Nanotubes. *Phys. Status Solidi B* **2006**, *243*, 3452–3457.
37. Maultzsch, J.; Reich, S.; Thomsen, C. Raman Scattering in Carbon Nanotubes Revisited. *Phys. Rev. B* **2002**, *65*, 233402.
38. Dresselhaus, M. S.; Jorio, A.; Souza Filho, A. G.; Saito, R. Defect Characterization in Graphene and Carbon Nanotubes Using Raman Spectroscopy. *Philos. Trans. R. Soc. A* **2010**, *368*, 5355–5377.
39. Sasikumar, K.; Keblinski, P. Effect of Chain Conformation in the Phonon Transport across a Si-Polyethylene Single-Molecule Covalent Junction. *J. Appl. Phys.* **2011**, *109*, 114307.
40. Strictly speaking, zeta potentials do not provide conclusive measures for molecular packing. Thus, we cannot entirely rule out the possibility of the surfactant packing effects.
41. Gunlycke, D.; Lawler, H. M.; White, C. T. Lattice Vibrations in Single-Wall Carbon Nanotubes. *Phys. Rev. B* **2008**, *77*, 014303.
42. Blochl, P. E. Projector Augmented-Wave Method. *Phys. Rev. B* **1994**, *50*, 17953.
43. Perdew, J. P.; Burke, K.; Ernzerhof, M. Generalized Gradient Approximation Made Simple. *Phys. Rev. Lett.* **1996**, *77*, 3865.
44. Kresse, G.; Joubert, D. From Ultrasoft Pseudopotentials to the Projector Augmented-Wave Method. *Phys. Rev. B* **1999**, *59*, 1758.
45. Hertel., T.; Moos, G. Electron-Phonon Interaction in Single-Wall Carbon Nanotubes: A Time-Domain Study. *Phys. Rev. Lett.* **2000**, *84*, 5002.